

REVIEWED

Selective Laser Sintering of Diamond Lattice Structures: Experimental Results and FEA Model Comparison

Clayton Neff¹, Neil Hopkinson², Nathan B. Crane¹

Affiliation: ¹University of South Florida, Tampa, FL; ² University of Sheffield, Sheffield, UK

Abstract

Nature utilizes multiple materials with varying properties to create high performance, integrated systems. In contrast, most additive manufacturing processes are limited to a small set of compatible materials to fabricate a device. However, the large geometric freedom of AM could be used to create the effect of multiple properties by creating lattice structures. Prior work has focused on using this concept to reduce weight in high stiffness structures. This paper will consider the use of a diamond lattice structures to create the effect of materials with a low elastic modulus materials. Low stiffness regions are advantageous for energy absorption, vibration isolation, and reduction of stress due to dimensional or temperature mismatches. The diamond lattice possesses Face-Centered-Cubic (FCC) elemental configuration possessing tetrahedral angles of 109° between elements. This allows for a pliable moment exerted on the structure yielding a flexible and energy absorbent arrangement. A range of devices was fabricated in Nylon 12 (PA 2200) through Laser Sintering (LS) process with variable element size (thickness) and unit cell size. The effective stiffness of the structures is compared as a function of these parameters and compared to numerical simulation. The results show the possibility of tuning the effective elastic modulus by over four orders of magnitude.

Introduction

Additive Manufacturing (AM) utilizes digital control over the material structure to create parts directly from digital models. This reduces the cost of low volume manufacturing by reducing or even eliminating the need for part-specific tooling. Additionally, the geometric freedom of AM processes, enable the fabrication of unique geometries and materials that would not otherwise be possible. While the application space for AM is growing dramatically, some AM applications are limited by the available materials. [1]

While AM processes provide very wide geometric freedom, the materials available on a particular machine or process are much more restricted. In a typical machine, only one structural material can be deposited in a single part. Additionally, the range of properties achievable across all materials used on a machine is often relatively limited. For example, a metal AM machine is often only capable of depositing metal structures for which the stiffness would vary by less than 3x across all feasible materials. While some polymer systems such as thermal extrusion can deposit composites that significantly increase the property range, many processes would benefit from being able to achieve a wider range of properties utilizing the existing materials.

One strategy for achieving this goal is to utilize the geometric freedom of AM to create meta-structures that can emulate the characteristics of other materials. Meta-structures enable substantial variation in properties from tuned Poisson's ratio [2] and modifications of thermal expansion [3], to varied stiffness. This work will focus on tuning the mechanical characteristics of the structure. Significant work has been done on utilizing truss structures in order to maintain high stiffness while decreasing weight, printing time, and/or material usage [4, 5, 6]. However, these

structures typically seek to maximize the stiffness of the final part. There is a need for alternative structures that could be used to create low-stiffness parts. Such a capability could eliminate the need for low elastic modulus materials like rubber or foam in some applications. While some work has been done with low stiffness 2D structures [7], little has been done with 3D structures. This paper, considers the range of properties that could be achieved using one such structure: *a diamond lattice*. This will build on prior work quantifying response of metallic diamond structures to impact loads [8] and exploring some of the design considerations for design of impact absorbing structures [9].

Diamond Lattice Structure & Topology

Lattice materials are a special case of cellular structures that permits more flexible control over the material structure [10]. The goal for lattice materials and cellular solids is to achieve unique material combinations properties with the capability of tuning properties such as elastic modulus, poisson's ratio, and density across a wide range by varying the structure. [11, 12, 13] One common goal is to utilize minimal material meanwhile functioning as multipurpose structures subject to application-specific stiffness and strength requirements. Minimal material translates to the lattice configuration consisting of low density, thus yielding a cellular solid that produces open space within the unit cell. Molecular structure of diamond has a unique Face Centered Cubic (FCC) unit cell containing 8 carbon atoms. It possesses exceptional geometry that presents an Atomic Packing Factor (ATP) equal to 0.34 which implies low relative density when comparing the ATP for FCC metals is 0.74 [14]. In creating a lattice structure based on this model, the atom centers become nodes. Adjacent nodes are connected together by struts. The size of the unit cell and the cross section of the struts determines the structure stiffness. Upon observing Figure 1 it can be seen that the lattice structure of diamond has no direct load paths within the unit cell generating a low density cellular solid that can be produced and manufactured in the meta-material design space.

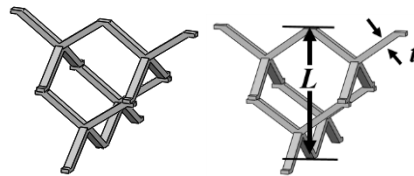


Figure 1: Unit cell structure of diamond

To explore how the diamond lattice would change mechanical properties, a wide range of unit cell lengths and thicknesses were manufactured through Laser Sintering (LS) and also analyzed in FEA. Unit cell lengths (L) were modified from 5 – 20 millimeters and thickness of the struts (t) varied from 0.5 – 2 millimeters, both parameters above in Figure 1. In order to understand how the parameters of unit cell length (L) and element thickness (t) vary the configuration of the diamond lattice, hence, directly the effective density of a combination of unit cell length (L) and thickness (t), figures of Solidworks models are rendered below. All of the laser-sintered diamond lattices and Solidworks models were (2x2x2) arrays of unit cells except where noted. The thickness (t) is the cross section thickness in the primary bending direction under a vertical load. The other cross section dimension was set to $1.25t$ to assure bending about a consistent axis. Figure 2 portrays the effect of thickness for a constant unit cell length of 10 mm. As the thickness is increased from

0.5 – 2 mm, the relative density of a diamond lattice with a 10 mm unit cell length mm increases significantly from 2.15 to 27.55 %.

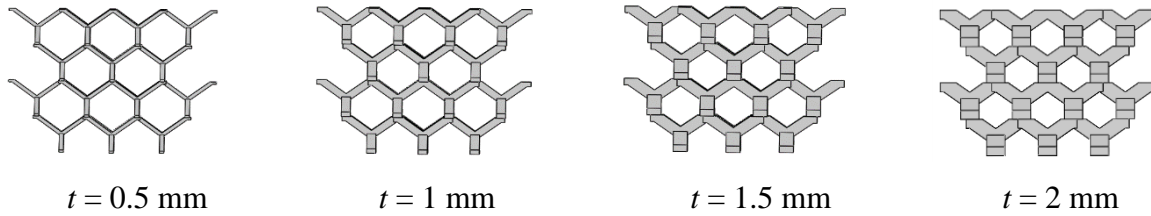


Figure 2: Variation of element thickness for unit cell length (L) of 10 mm

Now if the thickness is held constant while varying unit cell length, relative density is changed in an opposing manner. Figure 3 below exhibits a constant 1 mm thickness and fluctuating the unit cell length from 5 – 20 mm. Increasing the unit cell length in this fashion will decrease the relative density because increasing the distance from top to bottom of the unit cell makes the thickness of the struts proportionally smaller as seen below. It is worthy here to note the effect of relative density by adjusting the unit cell length and thickness for the reason that it directly manipulates the mechanical response of the diamond lattice.

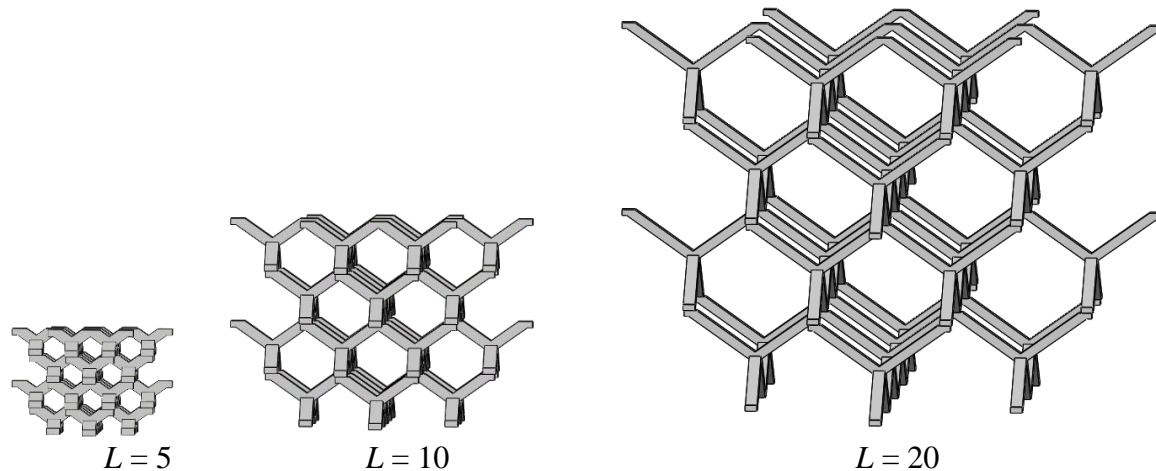


Figure 3: Variation of unit cell length for constant element thickness ($t = 1$ mm)

Experimental Research Method

Diamond lattice samples consisting of 2x2x2 arrays of diamond lattice cells were fabricated on an EOS Formiga P100 from PA2200 powder (50% virgin, 50% recycled) with a powderbed temperature of 170 C using 0.100 mm layers and 0.25 mm scan spacing. Scan speeds were 2500 mm/s on hatching and 1500 mm/s on the edges using 21W and 16W respectively. All parts were printed in the XYZ orientation as defined in ASTM F291-11. Parts were positioned at least 45 mm from the edges of the build volume and allowed to cool overnight before removal from the powder bed. The parts were cleaned with compressed air. Compression testing was performed on a Tinius Olsen Model H5K-S UTM 5kN testing system using the axis motion to calculate the applied strain. The displacement rate was adjusted to maintain a constant strain rate of 5%/min for all samples. Three to five samples were tested for each condition.

FEA Simulation Method

The compression tests were simulated using finite element analysis (FEA) in SolidWorks™. Boundary conditions were chosen to model the experimental compression testing with a fixed lower platen of a compression tester with an applied displacement on the top as illustrated in Figure 4 below. For the simulation, the diamond lattice's bottom pads were set to a zero displacement in the z-direction. The center contact point was fixed in all directions. This enabled the other bottom pads to slide in the x and y directions to accommodate transverse displacements. Motion in the x and y direction of bottom pads is characterized as “slipping” meaning the bottom pads would translate horizontally on a bottom plane as the diamond lattice is compressed. The top pads (seen in Figure 4 below) were set to a fixed displacement in the z-direction. A fixed displacement (δ) was set to simulate a certain desired strain for compression of the diamond lattices. For example, if the unit cell length of 10 mm (height of 20 mm for 2x2x2 array) was displaced 1 mm, this created an effective strain of 5%. The manufacturer supplied bulk properties values for PA 2200 (1.7 GPa for modulus, 0.394 for poisson's ratio, and 930 kg/m³) were used for the material properties in the simulation. A mesh convergence study was conducted for the various unit cell lengths and thickness combination to ensure refinement of the mesh was sufficient to have less than 1-2 % change in reaction forces when halving the element size. Large deflection conditions (Non-Linear Simulation) produced no more than 0.84 – 1.5 % deviation as linear analysis for 1% applied strains so linear results at 1% applied strains were used for all effective elastic modulus results reported below.

Representative resulting diamond lattice deformations are illustrated in Figure 5 with an applied displacement of (δ). The resultant force on the bottom pads was extracted to estimate the force of compression. After the resultant force was extracted it was converted to stress as the resultant force over the bottom plane area; the stress divided by the applied strain value produced an effective elastic modulus.

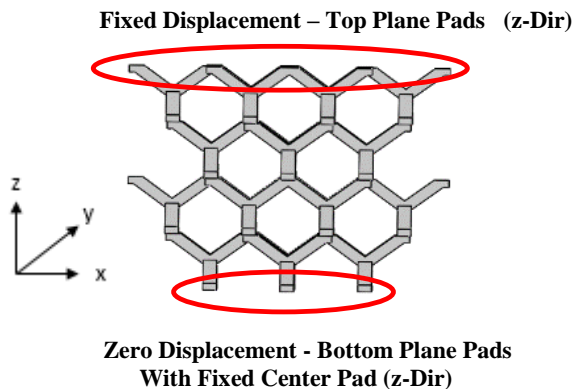


Figure 4: Boundary Conditions for Simulating Compression Testing of Diamond Lattice

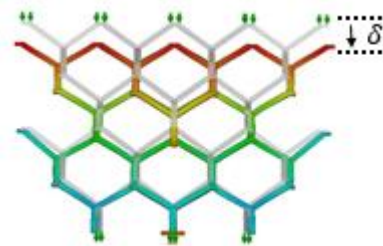


Figure 5: Plot of z Displacements in a Simulated Diamond Lattice under an Applied Displacement of (δ).

Additional simulations were performed to determine whether the compression stiffness of the 2x2x2 arrays of unit cells is representative of the bulk properties of 4x4x4 and 6x6x6 unit cell arrays as illustrated in Figure 6. The 4x4x4 and 6x6x6 models were cut into quarter models in an

effort to reduce simulation run time meanwhile obtaining accurate values of stiffness. Then symmetry conditions were applied to the quarter models (example of original and sliced 4x4x4 lattice shown in Figure 7 & 8 below) along with the same zero and fixed displacements as previously applied. Now however, the absolute fixed point was at the intersection of the two symmetry planes.

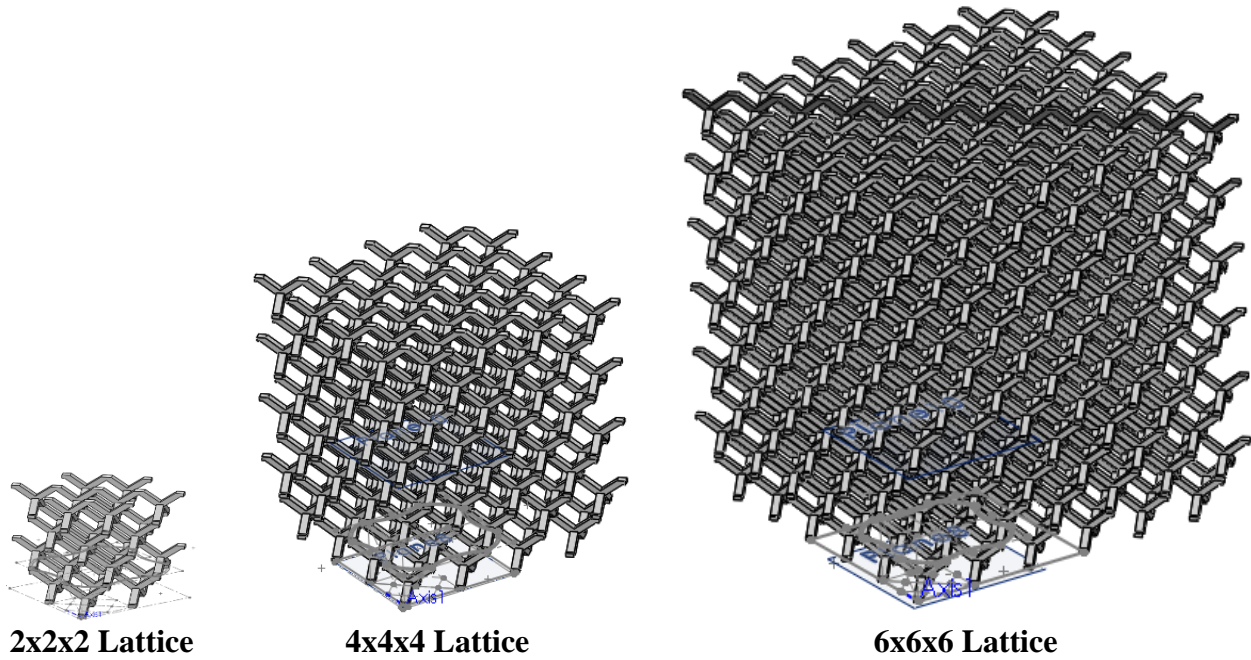


Figure 6: Diamond lattices with different numbers of unit cells.

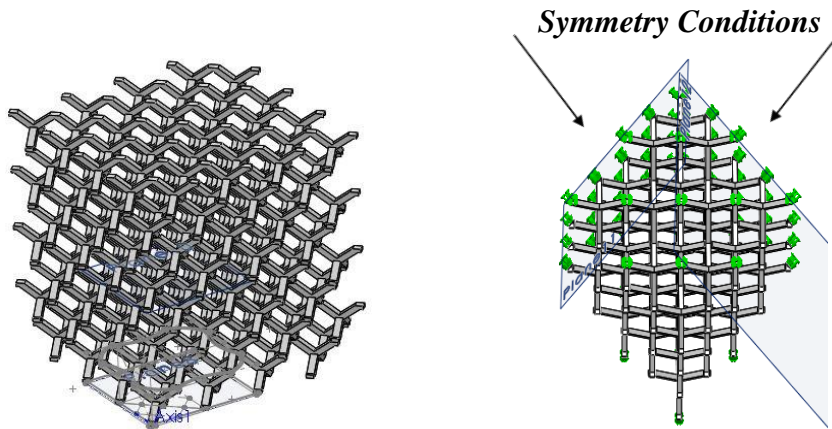


Figure 7: Original 4x4x4 Lattice

Figure #8: Simplified 4x4x4 unit cell diamond lattice model after applying symmetry conditions

The stiffness of the larger models was calculated as before and compared to the 2x2x2 unit cell values. The ratio of the effective modulus calculated by the 4x4x4 unit cell to that of the 2x2x2 case was compared as a function of the lattice unit cell length (L) to element size (t) ratios in Figure 9. The 4x4x4 unit cell was 4-7% less stiff for the t/L values of greatest interest. The error drops and reverses at larger t/L values, but the difference remains less than 7%. These values also have large relative densities (50-80%) which are considered outside of the cellular solid domain (<30% relative density). [15] For the region below 30% relative density, the change of elastic modulus has a max of 7% with most points floating between 4 – 6 % and the error from using the smaller test sample (2x2x2 unit cells) is minimal compared to the modulus variation of over 1000x across the geometries studied.

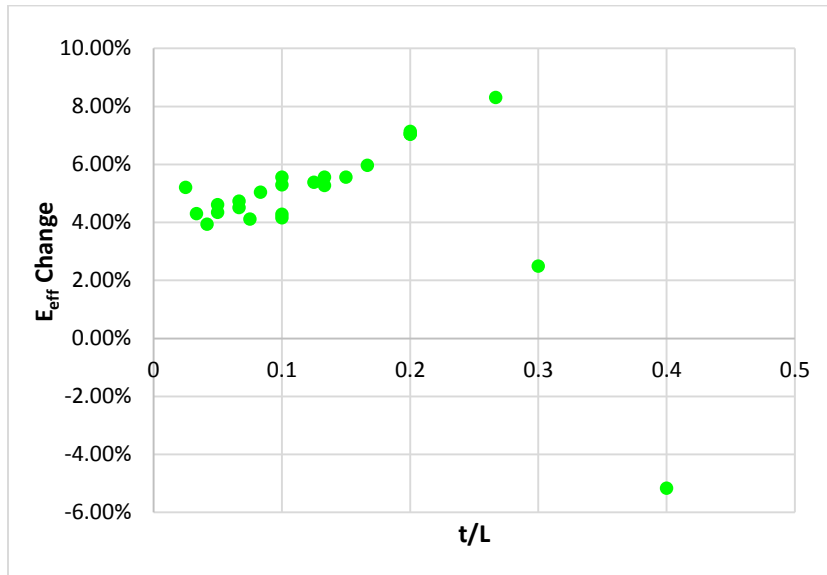


Figure 9: Percentage change of lattice stiffness with change of number of unit cells simulated from 2x2x2 to 4x4x4.

Results – FEA

The range of lattice conditions used in the simulations and in experiments are summarized in Table 1. Simulation results predict a change of elastic modulus proportional to the power of four for a given thickness and unit cell length. These trends are presented in Figures 10 & 11 below. The approximate fourth power relationship (varying from 3.83 – 4.07) with most of the exponents existing in the range of: 4 +/- 0.04. The results can be condensed to a relationship between the effective modulus and the ratio of element thickness to unit cell length (t/L). This relationship is represented in Figure 12 below. As (t/L) increases both the *density* and the stiffness increase as well. Since a thickness/length ratio (t/L) can be achieved with various combinations of unit cell length and thickness, other considerations such as process accuracy, build time can be utilized to select the specific parameters used to obtain to generate a diamond lattice for a specific application.

Table 1: Range of FEA and Experimental Stiffness for Size Parameters

Unit Cell Length (L) [mm]	Thickness (t) [mm]	(t/L)	FEA Simulation E_{eff} (MPa)	Experimentally Measured E_{eff} (MPa) with St. Dev.
5	0.5	0.1	3.59	0.504 ± 0.013
5	1.0	0.2	56.77	21.37 ± 0.483
5	1.5	0.3	263.51	N/A
5	2	0.4	708.33	N/A
7.5	0.5	0.067	0.69	0.099 ± 0.016
7.5	1.0	0.133	11.29	N/A
7.5	1.5	0.2	56.27	N/A
7.5	2	0.267	169.54	N/A
10	0.5	0.05	0.21	0.040 ± 0.0004
10	1.0	0.1	3.51	1.56 ± 0.010
10	1.5	0.15	17.97	10.93 ± 0.521
10	2	0.2	55.98	29.77 ± 1.585
12	0.5	0.042	0.10	N/A
12	1.0	0.083	1.66	0.76 ± 0.022
12	1.5	0.125	8.59	N/A
12	2	0.167	27.21	N/A
15	0.5	0.033	0.04	N/A
15	1.0	0.067	0.67	0.27 ± 0.007
15	1.5	0.1	3.47	N/A
15	2	0.133	11.10	N/A
20	0.5	0.025	0.012	N/A
20	1.0	0.05	0.209	0.80 ± 0.004
20	1.5	0.075	1.076	N/A
20	2	0.1	3.45	N/A

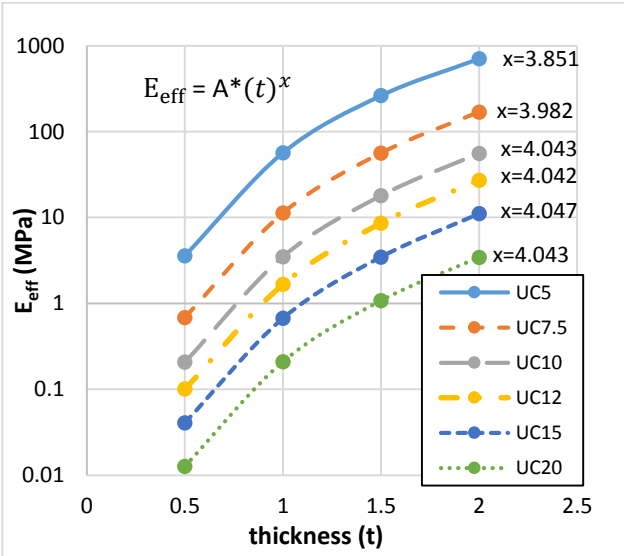


Figure 10: FEA calculated effective modulus vs element thickness (t)

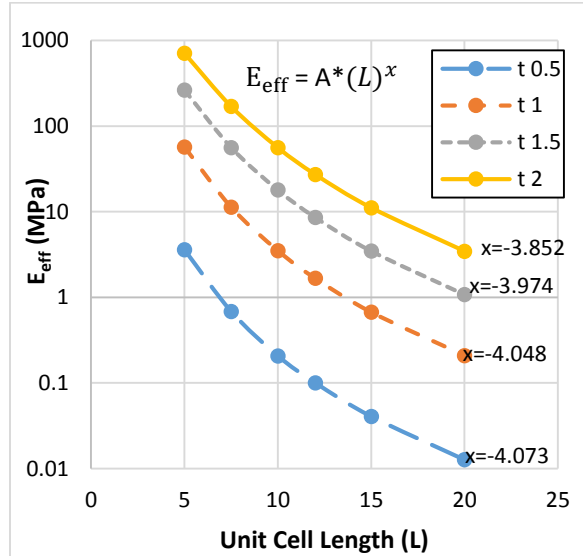


Figure 11: FEA calculated effective modulus vs diamond lattice unit cell length (L)

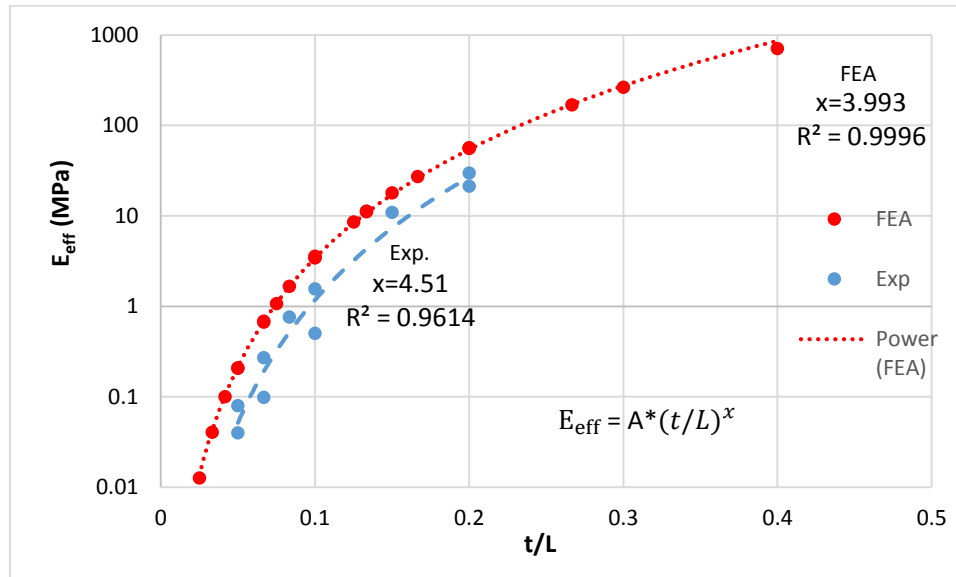


Figure 12: FEA calculated effective modulus of diamond lattice vs (t/L) compared to experimentally-measured effective modulus values and designed (t/L) .

Results – Experimental

The stiffness of the LS components measured from the compression test data is summarized in Table 1. Only the unit cell size of 10 mm has sufficient points to fit a relationship to effective modulus. It has an exponent significantly higher than predicted by the FEA (4.8). The experimental relationship with unit cell size is much closer to the FEA results with exponent of 3.7 and 4.2 for 0.5 mm and 1.0 mm element sizes respectively. It is also noted from Figures 13 & 14 that the effective modulus measured experimentally is substantially below the FEA predictions for all the tests cases though the difference is reduced at larger element size (t) values. This may be explained by the surface characteristics of LS components.

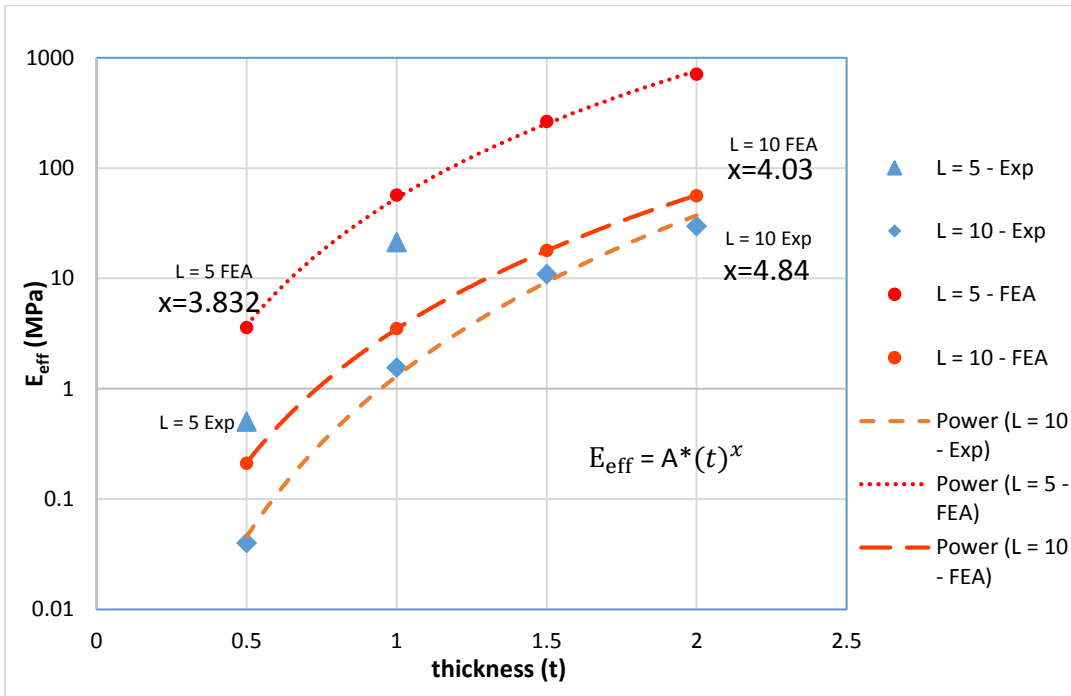


Figure 13: FEA vs Experimental values of the effective lattice modulus vs element thickness (t)

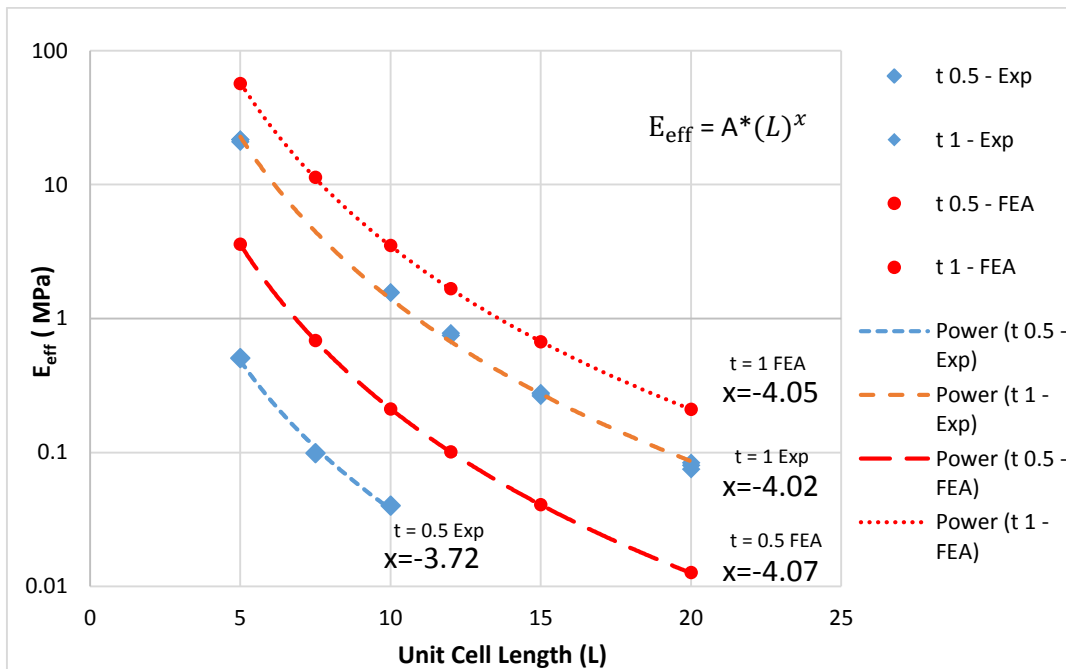


Figure 14: Comparison of FEA simulated to experimentally measured effective modulus vs unit cell length (L)

Laser sintered PA 2200 generally leaves partially densified layers on the outer surface of the part geometry that contributes to weight and thickness measurements, but does not influence strength and stiffness characteristics. This means that a designed part may not have the designed strength and stiffness intended because the measured thickness is not fully supporting the part geometry. Figure 15 below is an SEM image of the surface of a LS part cleaned with compressed air that illustrates the lightly compacted layers and surface roughness of laser sintered PA 2200.

These partially densified surface structures would substantially decrease the effective modulus of the thin printed elements to create a lower experimental measurements of effective modulus. Further, a consistent low density surface layer would have a larger impact on the thinner components and could produce the larger errors observed in the thinner element sizes. In order to further evaluate this possibility, the effective element size of each experimental element that would give the measured modulus values was calculated by scaling the FEA predictions based on the fourth order power relationship observed above.

The effective element size calculated for each experimental condition is summarized in Table 2. It is noted that the difference between the designed thickness and the effective thickness varies between 0.184 and 0.317 mm with an average of 0.211 mm for the variety of diamond lattices printed. The difference remains consistent across feature sizes from 0.5 mm to 1.5 mm. The the lightly compacted layers for laser sintered parts directly effects the performance of the diamond lattices in relation to the elastic modulus. From Table 2 it is indicated that the 0.5 mm thickness lattices have the largest difference of FEA to experimental elastic modulus and this is rationalized since the 0.211 mm lightly compacted layers are a much greater percentage of 35 – 41 % of designed thickness. As the thickness increases, the lightly compacted layers contribute to less of the designed thickness (close to 20%), thus reducing the divergence between experimental and simulated results.

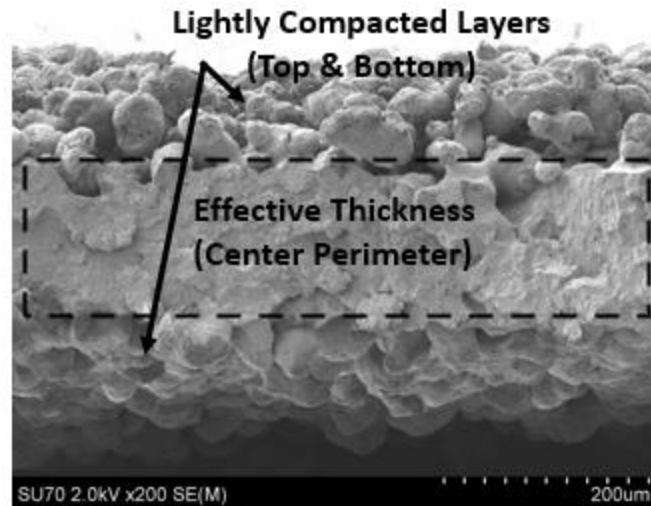


Figure 15: SEM image of laser sintered PA 2200 fracture surface illustrating surface structure of a single laser pass after air cleaning

Table 2 Effective thickness evaluation for FEA & experimental modulus deviation

Unit Cell Length (L)	Thickness (t)	Effective Thickness Error	Percentage of Designed Thickness	FEA/Exp E
5	0.5	0.204	41%	7.11
7.5	0.5	0.202	40%	6.94
10	0.5	0.177	35%	5.12
5	1	0.228	23%	2.66
10	1	0.193	19%	2.25
12	1	0.187	19%	2.29
15	1	0.213	21%	2.47
20	1	0.225	23%	2.63
10	1.5	0.184	12%	1.64
10	2	0.307	15%	1.88

Given the consistent magnitude of the difference between the design and effective thickness values, this could be applied as a design offset. The average of the effective thickness error calculated for all parts was subtracted from the design thickness to calculate an effective thickness. The effective modulus results are replotted in Figure 16. Since now the effective thickness is being applied for experimental results, the points are essentially shifted and promptly coincides to an enhanced resemblance of simulated data. The substantially improved agreement between FEA and experimental measurements with this correction suggests that this is an easy way to compensate for the process effects on material stiffness when designing for a target stiffness level. In practice, there may be additional sources of error including variations in material properties with thickness and errors in unit cell size, but these factors are unlikely to cause the large differences in experimental modulus values observed since unit cell size errors are much smaller and the lattice modulus value varies only linearly with material modulus of elasticity. Figure 17 plots the experimental and FEA modulus values against the (t/L) ratio, but utilizes the adjusted thickness values (design thickness minus average thickness error) for the experimental values. With this adjustment, the experimental and FEA results show good agreement. Careful assessment of these other error sources may yield further improvements in the prediction of lattice properties to guide design.

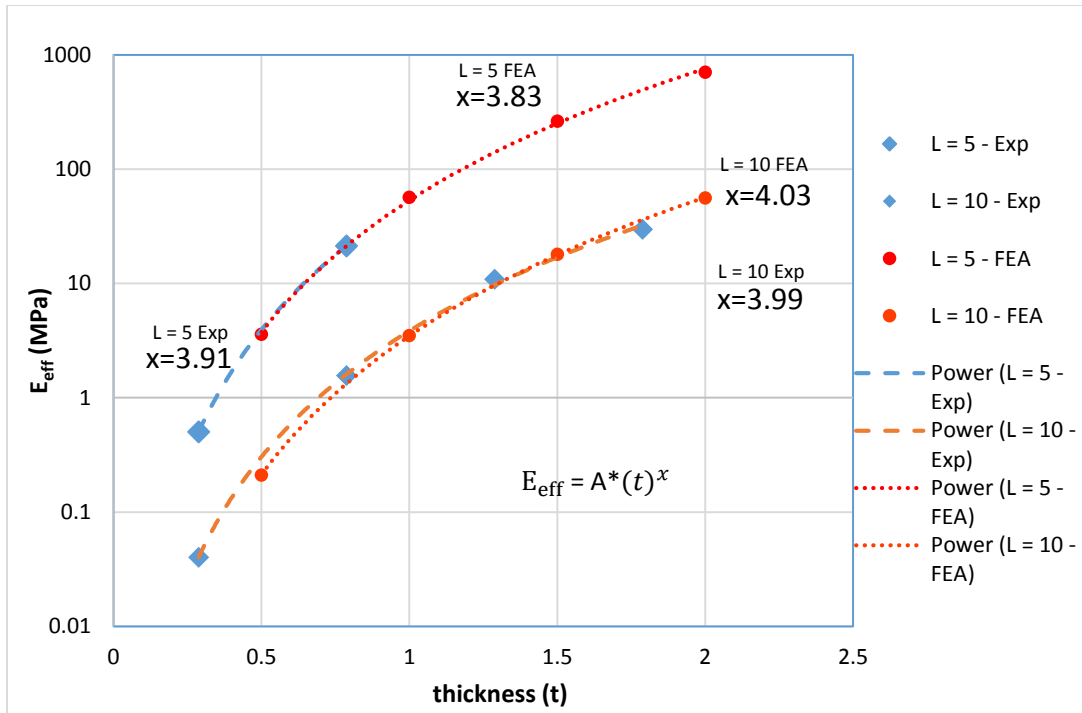


Figure 16: Comparison of effective lattice modulus predicted by FEA simulation vs experimental modulus measurements vs utilizing corrected thickness (t) values

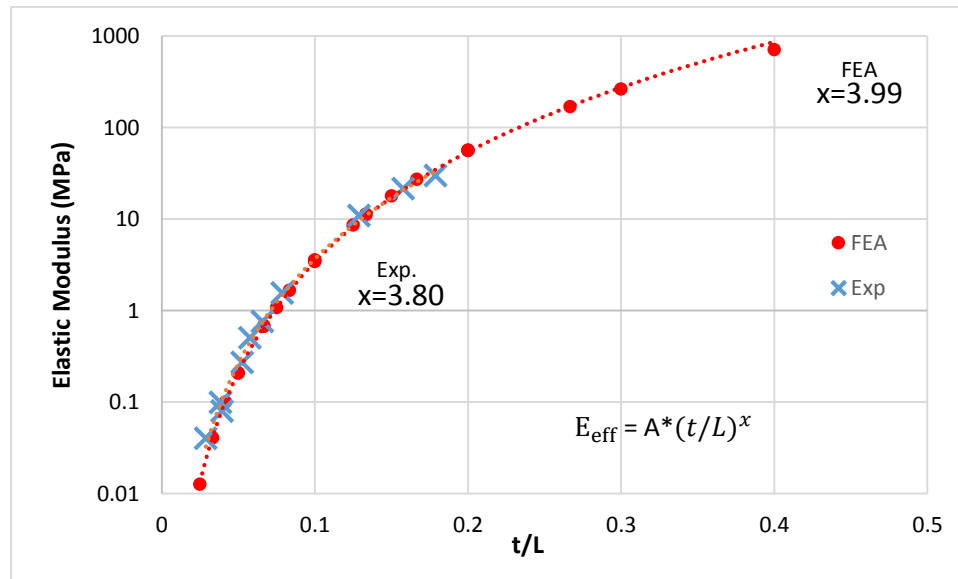


Figure 17: Simulation and experimental values of the effective elastic modulus measurements vs (t/L) utilizing the corrected thickness (t) values

As mentioned above, different combinations of thickness and unit cell length that produce the same (t/L) ratio for the diamond lattice configuration will have constant effective modulus and density values. Figure 18 presents a chart that can identify potential unit cell length and thickness for given stiffness and density. Along the dark lines are FEA values that are then extrapolated (dashed lines) to expand the amount of design space for diamond lattice parameters. The shaded triangular region is where the relative density limit of 30% is drawn as in that region design start to diverge from the realm of cellular solids. Additional limits are imposed by the process resolution constraints. The minimum thickness is the minimum feature size of the part—here taken as 0.5 mm. Within this region, t/L values can be selected to achieve the desired effective modulus values.

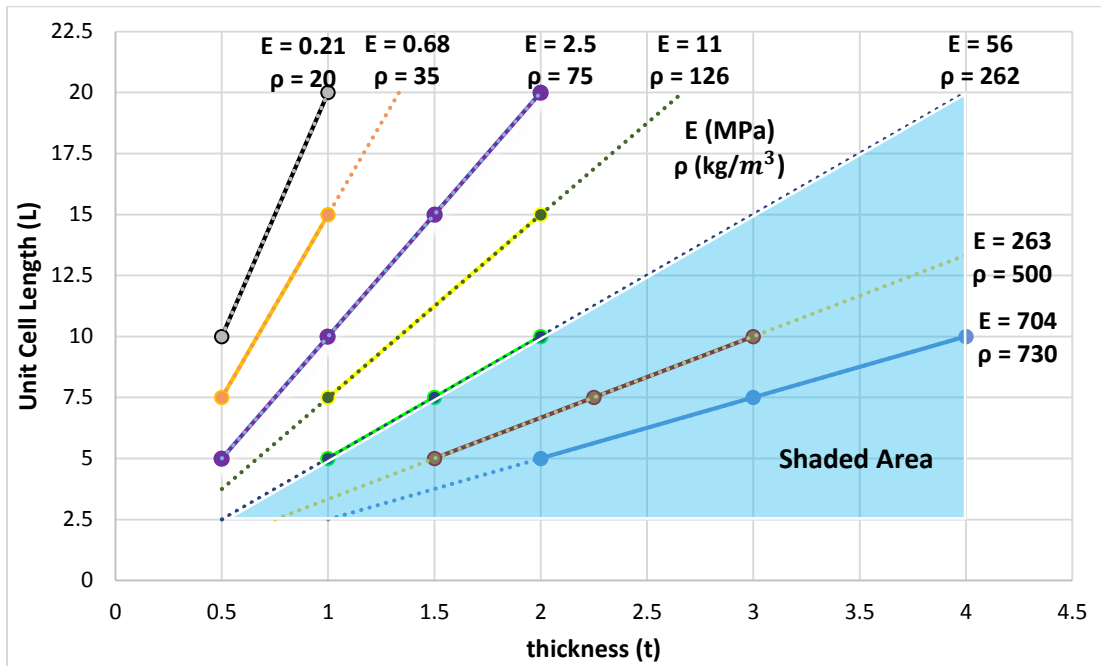


Figure 18: Plot of constant curvature/density lines as a function of unit cell and thickness dimensions

Conclusions

Meta-structured systems can create an effective “meta-material” with properties that can be tuned to specific design requirements. Generating meta-materials in the arrangement of diamond lattice has proven to produce structures that vary in effective elastic modulus over four orders of magnitude. The stiffness is shown to vary to the fourth power with the ratio of the element thickness to the unit cell size. This research also provides an effective error analysis for the thickness of laser sintered parts to assess the divergence of simulated and experimental results. Once an effective thickness was applied, the experimental results were in agreement with FEA.

References

1. I. Gibson, D. W. Rosen, B. Stucker, *Additive Manufacturing Technologies: Rapid Prototyping to Direct Digital Manufacturing*. Springer, New York, 2010.
2. A. L. Cooke, et al. "An investigation of the material properties of laser sintered parts incorporating conformal lattice structures (CLS™) technology". *24th International Solid Freeform Fabrication Symposium – An Additive Manufacturing Conference*, SFF 2013, August 12, 2013 – August 14, (University of Texas at Austin (freeform) , Austin, TX, United States, 2013) pp. 908-928.
3. N. M. A. Palumbo, et al. "Near-zero thermal expansivity 2-D lattice structures: Performance in terms of mass and mechanical properties". *Acta Materialia* 59, 2392-2403. 2011.
4. C. Yan, L. Hao, A. Hussein, D. Raymont. "Evaluations of cellular lattice structures manufactured using selective laser melting". *International Journal of Machine Tools & Manufacture*. 62(2012): 32-38.
5. V. S. Deshpande, N. A. Fleck, M. F. Ashby. "Effective properties of the octet-truss lattice material". *Journal of the Mechanics and Physics of Solids*. 49(2001): 1747-1769.
6. S. Tsopanos, R. A. W. Mines, S. McKown, Y. Shen, W. J. Cantwell, W. Brooks, C. J. Sutcliffe. "The Influence of Processing Parameters on the Mechanical Properties of Selectively Laser Melted Stainless Steel Microlattice Structures". *Journal of Manufacturing Science and Engineering*. 132(2010): 041011.
7. Guarav Gupta, JunJay Tan, and Carolyn Conner Seepersad. "Design and Freeform Fabrication of Compliant Cellular Materials with Graded Stiffness". *17th International Solid Freeform Fabrication Symposium – An Additive Manufacturing Conference*, SFF 2006, August 14, 2006 – August 16, (University of Texas at Austin (freeform) , Austin, TX, United States, 2013) pp. 908-928.
8. Ozdemira, Everth Hernandez-Nava, Andrew Tyas, Russell Goodall, "Quasi-static behavior and impact characteristics of micro-structured truss materials", *Proceeding of the 20th UK Conference of the Association for Computational Mechanics in Engineering*, the University of Manchester, Manchester, March 27-28, 2012.
9. J. Brennan-Craddock, et al. "The design of impact absorbing structures for additive manufacture". *Modern Practice in Stress and Vibration Analysis 2012*, MPSVA 2012, August 28, 2012 – August 31, (Institute of Physics Publishing, Glasgow, United Kingdom, 2012).
10. M. F. Ashby. "The properties of foams and lattices". *Philosophical Transactions of The Royal Society A*. 364(2006): 15-30.
11. J. Schwerdtfeger, P. Heintl, R. F. Singer, C. Korner. "Auxetic cellular structures through selective electron-beam melting". *Physics Status Solidi B*. 247(2010), 2:269-272.
12. L. E. Murr, S. M. Gaytan, F. Medina, E. Martinez, J. L. Martinez, D. H. Hernandez, B. I. Machado, D. A. Ramirez, R. B. Wicker. "Characterization of Ti-6Al-4V open cellular foams fabricated by additive manufacturing using electron beam melting". *Materials Science and Engineering A*. 527(2010): 1861-1868.
13. L. Yang, O. Harrysson, H. West, D. Cormier. "Compressive properties of Ti-6Al-4V auxetic mesh structures made by electron beam melting". *Acta Materialia*. 60(2012): 3370-3379.
14. Callister Jr., William D. *Materials Science and Engineering an Introduction, 7th Edn*. John Wiley & Sons, 2007. Print.
15. Gibson, L. J. and M. F. Ashby, 1997, *Cellular Solids: Structure and Properties*, Cambridge University Press, Cambridge, UK.